INDIAN INSTITUTE OF TECHNOLOGY KHARAGPUR

MASTER THESIS PROJECT - 1

Precise Measurements and Advanced Modeling of Barium Ion Polarizability

---

Author:
Pranay PANDEY

Supervisor:
Prof. Douglas Murray BARRETT and Prof. Sonjoy MAJUMDER

DEPARTMENT OF PHYSICS

November 28, 2024

INDIAN INSTITUTE OF TECHNOLOGY KHARAGPUR

Abstract

Prof. Douglas Murray BARRETT and Prof. Sonjoy MAJUMDER
Department of Physics

Intergrated BS and MS in Physics

Precise Measurements and Advanced Modeling of Barium Ion Polarizability

by Pranay PANDEY

This thesis presents a comprehensive study of the differential polarizability zero crossing in the Ba^+ ion clock transition using experimental measurements and theoretical modelling. The unique properties of the Ba^+ ion clock transition at 480 nm, particularly the emergence of a zero crossing in the differential polarizability, are investigated in detail. The theoretical underpinnings of this phenomenon, including the contributions from branching ratios, matrix elements, and higher-order effects estimated through perturbation theory, are discussed rigorously. The experimental setup, including using a stabilized 480 nm laser and the Pound-Drever-Hall technique, is described as the primary framework for this investigation. The results of this study contribute to the understanding of the polarizability behavior in Ba^+ ions and open up new possibilities for improving the performance of optical frequency standards and atomic clocks.

Acknowledgements

I would like to express my profound appreciation to my supervisors, Prof. Douglas Murray Barrett and Prof. Sonjoy Majumder, whose invaluable guidance, support, and encouragement have been instrumental in completing this thesis project. His profound knowledge, insightful feedback, and unwavering patience have constantly inspired me to explore new heights in my research. His mentorship has enriched this research project and greatly influenced my personal and professional growth. I am genuinely grateful for his dedication and the opportunity to learn from him.

Contents

Chapter 1

Introduction

1.1 Context

The groundbreaking discovery of the Ba+ ion's differential polarizability zero crossing provides significant insights into the field of atomic clock precision. The Ba+ ion, when subjected to a 480 nm laser, exhibits unique properties that can be exploited to improve the performance of optical frequency standards. Zero crossing in differential polarizability is crucial for mitigating electric field-induced shifts, commonly known as Stark shifts, which are a significant source of inaccuracy in atomic clocks.

Atomic clocks have revolutionized modern technology, offering timekeeping precision that underpins many advanced applications, such as satellite-based navigation, communication systems, and fundamental physics research. The Ba+ ion, with its favourable atomic properties, represents a promising candidate for developing highly accurate optical clocks. By identifying the conditions under which polarizability reaches zero, the study aims to enhance clock stability by reducing Stark shifts that affect atomic transitions. This research delves into the experimental measurement of the differential polarizability of Ba+ ions, highlighting the role of branching ratios, matrix elements, and perturbation theory in accurately modelling polarizability.

Advanced techniques such as the Pound-Drever-Hall (PDH) stabilization and a stabilized 480 nm laser allow for high-precision measurements, ultimately contributing to developing more reliable optical clocks. The findings of this study have profound implications for the future of atomic metrology, enabling more accurate timekeeping and potential applications in fields such as satellite-based navigation, quantum computing, and tests of fundamental physics.

1.2 Motivation

This study aims to characterize the differential polarizability zero crossing in the Ba+ ion clock transition through experimental and theoretical approaches. The primary objective is to accurately determine the conditions under which the zero crossing occurs and understand the underlying mechanisms contributing to this phenomenon. By investigating the effect of branching ratios, matrix elements, and perturbation theory on polarizability, this study aims to provide insights into how electric fields influence the Ba+ ion's energy levels and transition frequencies.

The motivation for this work stems from the need for more accurate atomic clocks,

which are crucial for many scientific and technological applications. Reducing electric field-induced shifts in optical frequency standards is critical to improving timekeeping accuracy. In addition to the experimental measurements, this study seeks to validate theoretical predictions and provide a deeper understanding of the observed behaviour. By rigorously explaining the results obtained from the experiments, this work aims to enhance the precision of Ba+-based optical clocks, thereby contributing to advancements in atomic metrology and fundamental research in atomic physics. The ultimate goal is to mitigate sources of inaccuracy in optical frequency standards and improve the performance of atomic clocks for a wide range of applications.

1.3 Objectives and Contributions

The specific objectives of this research are as follows:

- To experimentally measure the differential polarizability zero crossing in the Ba^+ ion clock transition at the 480 nm wavelength.
- To develop and apply advanced laser stabilization techniques, including PDH stabilization, to achieve high-precision measurements.
- To theoretically model the polarizability using perturbation theory, incorporating branching ratios and matrix elements to validate experimental findings.
- To comprehensively analyse the impact of polarizability zero crossing on minimizing Stark shifts and improving atomic clock performance.

The main contributions of this work include the experimental demonstration of the differential polarizability zero crossing for Ba^+ ions, the development of a high-precision experimental setup, and the validation of theoretical models. These contributions are expected to advance the field of atomic metrology by improving the accuracy and stability of Ba^+ optical clocks.

1.4 Problem Statement

One of the primary challenges in optical clock development is minimizing the electric field-induced Stark shifts that degrade clock precision. For the Ba+ ion, accurately determining the differential polarizability zero crossing at the 480 nm wavelength can help mitigate these effects. The main problem addressed in this study is to experimentally and theoretically identify the conditions under which the zero crossing occurs, thereby reducing the impact of external electric fields on the transition frequencies of the Ba+ ion. This requires an in-depth understanding of the interactions between the ion and applied fields and developing reliable experimental techniques for measuring these effects with high precision.

1.5 Scope

The scope of this study is primarily focused on the investigation of the differential polarizability zero crossing in the Ba+ ion clock transition using both experimental measurements and theoretical modelling. The study will use a 480 nm laser to measure polarizability, the application of electric fields, and the analysis of the resulting

effects on the transition frequency. In addition to experimental validation, the study aims to provide a rigorous theoretical perspective on the observed behaviour. However, it is essential to note that this study does not encompass all aspects of Ba+ ion research. The focus is specifically on the polarizability of zero crossing and its impact on atomic clock performance, and other potential applications of Ba+ ions, such as in quantum information processing, are beyond the scope of this work.

1.6 Limitations

Several limitations are relevant in the context of this study on the differential polarizability zero crossing in Ba+ ions. The experimental measurements are subject to uncertainties, including the precision of electric field control and laser stabilization, which can influence the accuracy of the results. Additionally, the theoretical modelling relies on approximations such as perturbation theory and branching ratios, which may introduce errors. Environmental factors, including temperature and pressure variations, can also affect the measurement outcomes. These limitations should be considered when interpreting the results and their implications for improving atomic clock performance.

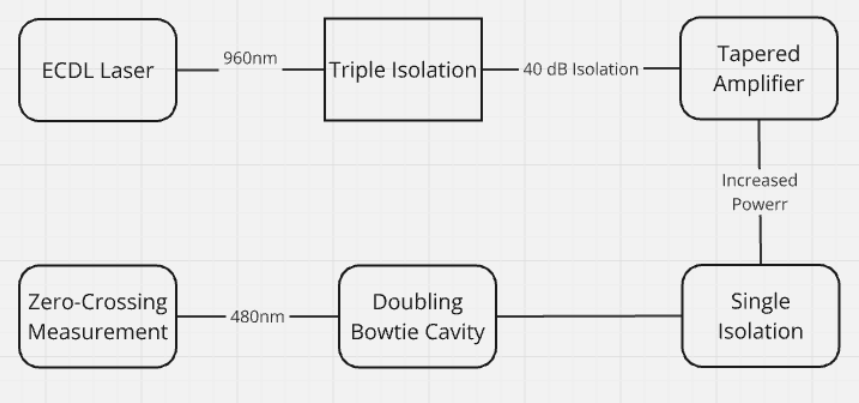

FIGURE 1.1: Experiment Schematic.

Chapter 2

Theoretical Formalism

2.1 Differential Polarizability of Ba^+

The polarizability of the Ba^+ ion plays a critical role in improving the precision of atomic clocks by mitigating electric field-induced Stark shifts, which are significant sources of inaccuracy. Understanding the differential polarizability $\Delta\alpha(\omega)$ helps control these shifts effectively, enhancing the performance of optical frequency standards Barrett, Arnold, and Safronova, 2019.

2.2 Differential Polarizability Model

As discussed in Barrett, Arnold, and Safronova, 2019, the differential polarizability of the Ba^+ clock transition can be written as:

$$\Delta\alpha_0(\omega) = \frac{c_{614}}{1-(\omega/\omega_{614})^2} - \frac{c_{455}}{1-(\omega/\omega_{455})^2} - \frac{c_{493}}{1-(\omega/\omega_{493})^2} + \frac{c_0}{1-(\omega/\omega_0)^2}, \quad (2.1)$$

where the first three terms are the contributions from the transitions at the indicated wavelengths, and the last term is an approximation to the remaining UV transitions and valence-core corrections that is accurate to second order in ω/ω_0, with the pole position ω_0 corresponding to an approximate wavelength of 222(5) nm as determined from theory Hoffman et al., 2013; Zhang et al., 2020. The constants c_k determine the strength of each pole, and we have:

$$c_{614} = \frac{1}{9}\frac{|\langle P_{3/2}\|r\|D_{5/2}\rangle|^2}{\omega_{614}}, \quad (2.2)$$

$$c_{455} = \frac{1}{9}\frac{|\langle P_{3/2}\|r\|S_{1/2}\rangle|^2}{\omega_{614}}\left(\frac{\omega_{455}}{\omega_{614}}\right)^3\frac{1-p}{p}, \quad (2.3)$$

$$c_{493} = \frac{1}{3}c_{455}\left(\frac{\omega_{455}}{\omega_{614}}\right)^4\frac{1-p}{p}, \quad (2.4)$$

$$c_{614} = \frac{1}{3}Rc_{493}\left(\frac{\omega_{455}}{\omega_{614}}\right)^4\frac{1-p}{p}, \quad (2.5)$$

p is a measured branching fraction reported in Zhang et al., 2020. We have also introduced the ratio:

$$R = \frac{c_{455}}{c_{493}} = \frac{|\langle P_{3/2}\|r\|S_{1/2}\rangle|^2}{|\langle P_{1/2}\|r\|S_{1/2}\rangle|^2}\frac{\omega_{493}}{\omega_{455}}, \quad (2.6)$$

for which calculations are expected to yield highly accurate assessments Chanu et al., 2020.

2.2.1 Model Simplification

Using the zero crossing near 650 nm defined by $\Delta\alpha_0(\omega_{650}) = 0$, we can write:

$$c_0 = \left[\frac{1-(\omega_{650}/\omega_0)^2}{1-(\omega_{650}/\omega_{493})^2} + \frac{1-(\omega_{650}/\omega_0)^2}{1-(\omega_{650}/\omega_{455})^2}R - \frac{1-(\omega_{650}/\omega_0)^2}{1-(\omega_{650}/\omega_{614})^2}RP\right] c_{493}, \quad (2.7)$$

which can be used to replace the variable c_0 with an experimentally measured value of ω_{650} Chanu et al., 2020. As the approximating UV pole is accurate to second order in ω/ω_0 and captures a good portion of the fourth order terms, we expect the model to be accurate near the zero crossing near 480 nm defined by $\Delta\alpha_0(\omega_{480}) = 0$.

We can then use this relation to write $R = R(\omega_{480}, \omega_{650}, P, \omega_0)$, which may be used to eliminate R from the model. Insofar as the model is accurate, $R = R(\omega_{480}, \omega_{650}, P, \omega_0)$ can thus be deduced from the measured values of ω_{480}, ω_{650}, P, and the estimated value of ω_0. This leads to a model that is proportional to c_{493}, which is determined by a single measurable matrix element, with the constant of proportionality determined by two measured zero crossings, a single measured branching fraction, and weakly dependent on a theoretical estimate of the approximating pole position.

2.2.2 Validation and Comparisons

To investigate the validity of the model and its predictive power for R and $\Delta\alpha_0(0)$, we use the atomic structure calculations given in Barrett, Arnold, and Safronova, 2019 and the corresponding differential polarizability as a possible instance of the actual atom. Using the parameters ω_{480}, ω_{650}, P, c_{493}, and ω_0 as determined from the given instance, we compare the values of R and $\Delta\alpha_0(0)$ determined from the constructed model to the instance of the real atom.

We compare three different methods to determine ω_0 by agreement with the value and second derivative at $\omega = 0$, agreement at $\omega = 0$ and ω_{650}, and agreement at $\omega = 0$ and ω_{480}. The fractional errors for each case are tabulated in Table 2.1.

ω_0 (au)	λ_0 (nm)	$\delta R/R$ ($\times 10^{-4}$)	$\delta\Delta\alpha_0(0)/\Delta\alpha_0(0)$ ($\times 10^{-4}$)
0.2054	221.8	-0.51	-2.38
0.2049	222.4	-0.34	-0.54
0.2043	223.0	-0.16	-1.23

TABLE 2.1: Fractional errors between model and atomic structure calculations for different methods of determining ω_0. Fractional errors are relative to 10^{-4}.

2.2.3 Conclusions

The differential polarizability model for Ba^+ presented here provides a comprehensive approach for determining the constants governing the polarizability behaviour across a wide frequency range. By utilizing the zero crossings at 480 nm and 650 nm and atomic structure calculations Le Kien, Schneeweiss, and Rauschenbeutel, 2013; Hoffman et al., 2013, we can derive the matrix element ratio R with high accuracy.

Further refinement of the model parameters, based on improved experimental precision, will continue to reduce the uncertainties associated with the clock transition of Ba^+.

2.3 Importance of Zero Crossing Measurements

Zero crossings in the differential polarizability are crucial for accurately determining various parameters in the polarizability model for Ba^+ Barrett, Arnold, and Safronova, 2019. The differential polarizability ($\Delta\alpha(\omega)$) is critical in reducing Stark shifts in atomic clocks, enhancing their precision.

The two main zero crossings for Ba^+ are observed at approximately 480 nm and 650 nm. These measurements are crucial for constructing an accurate model of the differential polarizability and minimizing uncertainties in clock transitions Zhang et al., 2020.

Key Aspects of Zero Crossing Measurements

1. **Parameter Determination**:
   The zero crossings at 480 nm and 650 nm help to determine key parameters like the ratio of matrix elements R, affecting the overall polarizability behaviour. The ratio R can be mathematically expressed as:

   $$R = R(\omega_{480}, \omega_{650}, P, \omega_0) \tag{2.8}$$

   Where:

   - ω_{480} and ω_{650} are the zero crossing frequencies at 480 nm and 650 nm.
   - P represents the branching fraction.
   - ω_0 represents the UV pole position.

   The branching fraction (P) and the UV pole position (ω_0) are additional important parameters influenced by the zero crossing measurements. We can refine the polarizability model to eliminate or adjust constants like R and c_0 by knowing the zero crossing at these two specific wavelengths. This improves the accuracy of the calculated polarizability and allows for a more precise assessment of how external electric fields affect Ba^+.

2. **Role in Determining the Strength of UV Contributions**:
   The zero crossing at 480 nm helps determine the strength of the contributions from UV transitions. The c_0 constant, representing the effect of UV transitions, can be adjusted based on the experimentally determined zero crossing. This results in a better alignment between the theoretical polarizability model and the experimental data, reducing uncertainties in the frequency standards used in atomic clocks.

3. **Simplification of the Polarizability Model**:
   By measuring the zero crossings, the model can be simplified, which makes the determination of parameters such as the matrix element ratios and the strengths of various transitions much easier. Specifically, when the zero crossing is experimentally determined, constants such as R and c_0 can be eliminated or precisely defined. This improves the alignment of theoretical models with

experimental observations, ultimately leading to more reliable and accurate clock measurements.

The differential polarizability equation is given by:

$$\Delta\alpha_0(\omega) = \frac{c_{614}}{1-(\omega/\omega_{614})^2} - \frac{c_{455}}{1-(\omega/\omega_{455})^2} - \frac{c_{493}}{1-(\omega/\omega_{493})^2} + \frac{c_0}{1-(\omega/\omega_0)^2} \quad (2.9)$$

Where:

- c_{614}, c_{455}, and c_{493} represent the contributions from transitions at 614 nm, 455 nm, and 493 nm, respectively.
- c_0 represents the contributions from UV transitions.
- The pole position ω_0 is theoretically estimated around 222 nm, accounting for second-order corrections and higher-order terms.

Using the experimentally determined zero crossings at 480 nm and 650 nm, we can effectively determine parameters like c_0 and R. This experimental data allows us to adjust the theoretical polarizability curve to match real-world observations, thereby minimizing discrepancies and reducing uncertainties in Stark shift calculations.

2.4 AC Stark Shift and Magic Wavelengths

The AC Stark shift and magic wavelengths are key elements in controlling polarizability-induced frequency shifts in Ba^+. As discussed in Barrett, Arnold, and Safronova, 2019; Hoffman et al., 2013; Le Kien, Schneeweiss, and Rauschenbeutel, 2013, the magic wavelength near 653 nm ensures minimal perturbation to the clock transition, significantly enhancing precision.

The AC Stark shift refers to the perturbation in the energy levels of an ion caused by an external oscillating electric field. This shift affects the clock transition frequency, impacting the precision of optical atomic clocks. The second-order Stark shift can be described by:

$$\delta E_a^{(2)} = -\frac{1}{2} E_L^2 \alpha_a(\omega) \quad (2.10)$$

Where:

- $\delta E_a^{(2)}$: Second-order Stark shift for atomic state $|a\rangle$.
- E_L: Amplitude of the applied electric field.
- $\alpha_a(\omega)$: Frequency-dependent polarizability of the atomic state.

In Ba^+ ($J = 1/2$), the Stark shift includes only scalar (α_s) and vector (α_v) components, as the tensor component (α_T) vanishes due to selection rules. The scalar component represents the average effect of the electric field, while the vector component depends on the orientation between the electric field and the quantization axis.

Magic Wavelength The "magic wavelength" is a specific wavelength where the AC Stark shifts of the clock states cancel each other out, minimizing frequency shifts. For Ba^+, the magic wavelength is identified near 653 nm (459.1614 THz). At this wavelength, the differential scalar polarizability ($\Delta\alpha_0(\omega)$) becomes zero, resulting in negligible shifts between clock states. This ensures higher stability and accuracy for the clock frequency, as both states experience identical Stark shifts, reducing sensitivity to external electric field fluctuations.

Experimental Techniques and Impact To identify the magic wavelength, experiments involve averaging over the Zeeman sublevels to cancel linear Zeeman shifts and determine the centre frequency accurately. Identifying this magic wavelength minimizes systematic uncertainties, such as those induced by electric fields, which is crucial for achieving precise frequency measurements in Ba^+-based optical clocks.

Summary The AC Stark shift and magic wavelength concepts are key to improving Ba^+ optical clock performance. The impact of electric field-induced frequency shifts is minimised by tuning the clock transition to the magic wavelength (653 nm), enhancing stability and precision. This optimization reduces systematic uncertainties, thereby contributing significantly to the accuracy of Ba^+ optical clocks.

2.5 Third-Order Effects and Hyperfine Interaction

The third-order hyperfine interactions and their effects on differential polarizability are further discussed in Arnold et al., 2019. These corrections play an important role in understanding higher-order contributions to Stark shifts in Ba^+.

In addition to the second-order AC Stark shift, third-order effects must be considered to accurately model the differential polarizability in Ba^+. These third-order perturbations involve interactions between the hyperfine structure (HFS) and the electric field, resulting in a more precise energy correction, particularly for precision measurements.

The hyperfine interaction is expressed as:

$$V_{\text{hfs}} = \mu \cdot B \tag{2.11}$$

Where:

- V_{hfs} represents the hyperfine interaction.
- μ is the nuclear magnetic moment.
- B is the magnetic field produced by the electron cloud.

Third-Order Perturbation Theory in Ba^+ The third-order Stark shift correction, denoted as $\delta E^{(3)}$, involves contributions from different topological arrangements of hyperfine and electric dipole interactions, labelled top, centre, bottom, and normalization terms. In this context:

- **Top Position ($T(\omega)$)**: Involves contributions where the hyperfine interaction occurs before the electric dipole interaction, with subsequent coupling to the electric field.

- **Center Position ($C(\omega)$)**: Describes configurations where the hyperfine interaction occurs between two electric dipole interactions.
- **Bottom Position ($B(\omega)$)**: Involves contributions similar to the top position but with conjugate terms.
- **Normalization Terms ($O(\omega)$)**: Accounts for the overall normalization effect due to multiple perturbative interactions.

These contributions collectively define the third-order dynamic Stark shift:

$$\delta E_a^{(3)} = \sum_{b,c\neq a} \frac{V_{ab}V_{bc}V_{ca}}{(E_b^{(0)} - E_a^{(0)})(E_c^{(0)} - E_a^{(0)})} - V_{aa} \sum_{b\neq a} \frac{V_{ab}V_{ba}}{(E_b^{(0)} - E_a^{(0)})^2} \tag{2.12}$$

Where a, b, and c are dressed atomic states, and V_{ij} represents the matrix elements of the interaction operator between states i and j.

The Role of Hyperfine Interactions The hyperfine interaction, V_{hfs}, involves coupling the nuclear magnetic moment and the electronic magnetic dipole. This coupling contributes additional terms in the perturbative expansion that must be accounted for when evaluating the total energy shift.

The hyperfine contribution is described as:

$$V_{\text{hfs}} = (\mu \cdot T^{(1)}) \tag{2.13}$$

$T^{(1)}$ is a rank-1 irreducible tensor operator acting on the electronic coordinates. The components of this operator are expressed as:

$$T_\lambda^{(1)} = -\frac{|e|}{4\pi\epsilon_0} i\sqrt{2} \left(\alpha \cdot C_{1\lambda}^{(0)}(r)\right) \frac{c}{r^2} \tag{2.14}$$

In this expression:

- α represents the Dirac matrices.
- $C_{1\lambda}^{(0)}(r)$ are the normalized vector spherical harmonics.
- The term $\frac{|e|}{4\pi\epsilon_0}$ is a coupling constant that defines the strength of the magnetic interaction.

2.5.1 Impact on Differential Polarizability

The hyperfine interactions play an active role in precision measurements. For Ba^+, the third-order perturbations involving hyperfine interactions are essential for accurately predicting differential polarizabilities. These effects become particularly significant for higher-order components that a simple second-order analysis cannot capture.

The third-order correction is also expressed in contributions from diagrams where the hyperfine interaction appears at different positions. These diagrams (a top, centre, bottom) indicate different ways the hyperfine and electric dipole interactions can combine, and their combined effect contributes to the overall correction.

Practically, incorporating these corrections helps eliminate discrepancies between theoretical and experimental measurements. The third-order corrections are crucial for minimizing uncertainties, especially in Ba^+ optical clocks, where even small shifts in polarizability can significantly affect clock accuracy.

Summary In Ba^+, third-order effects involving hyperfine interactions are vital to obtaining accurate models of differential polarizability. The third-order corrections involve contributions from various interaction diagrams, accounting for hyperfine and electric field couplings. This detailed modelling allows for a more precise determination of energy shifts, improving the performance of atomic clocks based on Ba^+.

2.6 Evaluation of Polarizability Contributions

Many-body corrections such as those discussed in Barrett, Arnold, and Safronova, 2019; Barrett, Arnold, and Safronova, 2019 are used to evaluate the polarizability contributions accurately. These advanced techniques provide a precise understanding of the interactions contributing to the differential polarizability of Ba^+.

To accurately evaluate the polarizability contributions of Ba^+, a comprehensive approach involving relativistic many-body theory is employed. This approach includes the following steps:

1. Relativistic Hartree-Fock (RHF) Calculations The first step in determining the polarizability of Ba^+ is to compute the electronic structure using relativistic Hartree-Fock (RHF) calculations. In the RHF method, the initial approximation is performed for the closed-shell atomic core, with the valence electron removed. This "frozen-core" approximation provides the basis for understanding the electronic configuration and is critical to calculating the wavefunctions of each electron, taking into account relativistic effects, which are especially important for heavier elements like Ba^+.

The RHF method essentially provides the unperturbed wavefunction, which is an eigenstate of the RHF Hamiltonian:

$$H_0\psi_0 = \epsilon_0\psi_0 \tag{2.15}$$

2. Correlation Effects via Brueckner Orbitals The RHF results are then refined by incorporating many-body effects using Brueckner orbitals. These orbitals are built using the correlation potential Σ, which modifies the Hamiltonian to account for two primary effects:

- **Screening of the Coulomb Interaction**: The effect of the surrounding electrons on the interaction between any two electrons is considered, effectively "screening" the Coulomb force.
- **Hole-Particle Interactions**: The interaction between an electron vacancy (hole) and the other electrons is also accounted for.

The correlation potential Σ is computed using Green's function techniques and summation over the complete set of states. The Brueckner orbitals are derived by treating Σ as a perturbation added to the RHF Hamiltonian:

$$H_{\text{eff}} = H_0 + \Sigma \tag{2.16}$$

Brueckner orbitals corresponding to the lowest valence states are considered good approximations of the real physical states and are used to calculate polarizability contributions in the summation of matrix elements.

3. Correlation Potential (Σ) The correlation potential Σ plays a key role in accurately modelling the electron correlations that influence polarizability. This potential modifies the Hamiltonian by including corrections for:

- **Screening Effects**: These effects consider how an electron's movement is influenced by other electrons, effectively screening the Coulomb interaction.
- **Hole-Particle Interactions**: These interactions describe the effects between an electron and a vacant state (hole) within the electronic structure.

The correlation potential Σ is calculated to all orders to ensure accuracy, using the B-spline technique to construct the necessary basis. The orbitals are expressed as a combination of B-splines and eigenstates of the RHF Hamiltonian with correlation potential modifications. These are known as Brueckner orbitals and are used to calculate the contributions to overall polarizability.

Additionally, the correlation potential is sometimes rescaled by a parameter λ to fit experimental energy values exactly. This rescaling further improves the match between theoretical predictions and experimental observations. For Ba^+, the rescaling parameters for different orbital angular momentum states (s, p, d) are close to unity, indicating minimal adjustment is needed for accurate predictions.

4. Incorporation of Many-Body Corrections Correlation corrections are included via the linearized coupled-cluster (LCC) method to further enhance the accuracy of the polarizability calculations. The LCC method incorporates:

- **Single-Double Excitations (SD)**: This approach includes the effect of excitations involving one or two electrons, which are crucial for accurately describing the electron correlation.
- **Partial Triple Contributions (SDpT)**: Some contributions from triple excitations are also included to account for higher-order effects.

These corrections are incorporated iteratively, leading to refined Brueckner orbitals that improve the calculation of polarizability matrix elements. Different methods, such as the Dirac Hartree-Fock (DHF) and random phase approximation (RPA), are also used to demonstrate the size and importance of correlation corrections.

Summary Evaluating the polarizability contributions in Ba^+ involves multiple sophisticated techniques:

- The **RHF method** provides the unperturbed wavefunctions.
- The **Brueckner orbitals** are obtained by applying the correlation potential, Σ, which incorporates screening and hole-particle interactions.
- The **correlation potential** is used to correct the Hamiltonian for many-body effects, and rescaling Σ helps align theoretical predictions with experimental results.
- The **linearized coupled-cluster method** (LCC) further improves the accuracy by including single, double, and partial triple excitations.

These steps collectively ensure that the contributions to polarizability are accurately evaluated, significantly improving the precision of Ba^+ optical clock frequency measurements.

2.7 Theoretical Model Validation and Experimental Comparisons

The experimental validation of the polarizability model, especially using the zero crossings and other parameters, ensures the reliability of the predictions Zhang et al., 2020; Chanu et al., 2020.

The validation of the theoretical model for the polarizability of Ba^+ involves comparing theoretical predictions with experimentally determined zero crossings at wavelengths near 480 nm and 650 nm. These zero crossings are essential because they provide direct information that can be used to adjust key model parameters such as branching fractions, matrix elements, and the UV pole contribution (c_0). These adjustments aim to improve the model's accuracy in predicting differential polarizability.

Experimental Zero Crossing Measurements Two significant zero crossings of the differential polarizability are experimentally measured at 480 nm and 650 nm to validate the theoretical model. The zero crossing is where the differential polarizability, denoted as $\Delta\alpha(\omega)$, equals zero, indicating that the polarizability-induced frequency shifts are minimized. This is crucial in reducing uncertainties in optical frequency standards, making these measurements vital for accurate atomic clock operation.

The zero crossing at 650 nm determines the UV pole contribution, c_0. Specifically, this zero crossing allows for replacing the variable c_0 in the model with an experimentally measured value:

$$c_0 = \left[\frac{1-(\omega_{650}/\omega_0)^2}{1-(\omega_{650}/\omega_{493})^2} + \frac{1-(\omega_{650}/\omega_0)^2}{1-(\omega_{650}/\omega_{455})^2}R - \frac{1-(\omega_{650}/\omega_0)^2}{1-(\omega_{650}/\omega_{614})^2}RP\right] c_{493} \quad (2.17)$$

Where ω_{650} is the frequency corresponding to the zero crossing at 650 nm, and ω_0 is the UV pole position, approximately 222 nm as estimated from theory.

Determining the Ratio of Matrix Elements R The experimentally determined zero crossings also help determine the ratio of matrix elements R, which plays a crucial role in the polarizability model. This ratio, R, can be expressed as:

$$R = R(\omega_{480}, \omega_{650}, P, \omega_0) \quad (2.18)$$

where P is the branching fraction, and ω_0 is the UV pole position. By measuring the zero crossings at 480 nm and 650 nm, the value of R can be deduced, which in turn helps adjust the model parameters. Once R is determined, it is possible to use this information to eliminate R from the model, leading to a model that is proportional to c_{493}, determined by a single measurable matrix element. This allows the constant of proportionality to be determined by two measured zero crossings, a single measured branching fraction, and an estimate of the UV pole position.

Model Validation through Comparisons The theoretical model is validated by comparing it with experimental data and ensuring that it accurately predicts the values of $\Delta\alpha(\omega)$. The comparison involves using atomic structure calculations for Ba^+, representing the differential polarizability as a real atom instance. For each instance, the parameters ω_{480}, ω_{650}, P, and c_{493} are well-defined, while ω_0 is subject to some interpretation.

The comparison is carried out by adjusting the parameters c_0 and ω_0 in different ways, such as:

- Agreement of the value and second derivative at $\omega = 0$
- Agreement at $\omega = 0$ and ω_{650}
- Agreement at $\omega = 0$ and ω_{480}

Each of these adjustments gives slightly different values for R and $\Delta\alpha(0)$, which are then tabulated to determine the model's accuracy. The smallest error for $\Delta\alpha(0)$ occurs when the UV pole approximation agrees at ω_{650}. In contrast, the smallest error for R occurs when the approximation agrees at ω_{480}, consistent with the model's expected behaviour.

Uncertainty and Contributions to Error The validation also involves quantifying the uncertainties in the model's predictions. The primary contributions to the uncertainty come from:

- Measurements of the zero crossings at 480 nm and 650 nm
- The determination of c_{493}
- The theoretical estimate of the UV pole position, ω_0

The uncertainties associated with these measurements are considered much smaller than those in the theoretical estimates, so the experimental data can be used to adjust the model parameters accurately. The fractional error between the model and atomic structure calculations for different methods of determining ω_0 is on the order of 10^{-4}, which shows good agreement between the theoretical model and experimental measurements.

Summary The validation of the theoretical model for Ba^+ polarizability involves a combination of experimental measurements and theoretical adjustments. By accurately determining the zero crossings at 480 nm and 650 nm, it is possible to adjust key parameters in the model, such as the UV pole contribution and the ratio of matrix elements. The comparison between theoretical predictions and experimental data demonstrates that the model can accurately describe the differential polarizability, leading to improved accuracy in optical clock performance.

2.8 Summary of Theoretical Findings

The theoretical investigation into Ba^+ polarizability provides a detailed understanding of the interactions and corrections that are crucial for enhancing the precision of optical frequency standards:

- **Second-Order Effects**: The AC Stark shift, primarily influenced by scalar and vector polarizability components, describes how the energy levels of Ba^+ respond to external electric fields. This understanding helps accurately model the ion's response, essential for mitigating frequency shifts in atomic clocks.

- **Zero Crossings**: The experimentally observed zero crossings at 480 nm and 650 nm are pivotal for fine-tuning the polarizability model. These zero crossings help determine key parameters like matrix element ratios and the contributions from ultraviolet transitions. Accurately capturing these points ensures that theoretical predictions align with experimental results, reducing clock frequency uncertainties.
- **Higher-Order Corrections**: Third-order hyperfine interactions are critical for achieving high precision beyond the second-order effects. These corrections consider the intricate coupling between the nuclear magnetic moment and the electronic magnetic dipole, refining the model to better match experimental data. Such higher-order corrections are essential when dealing with minute discrepancies that can significantly impact clock accuracy.

By identifying and measuring these zero crossings, Stark shifts can be minimized, improving stability and accuracy in Ba^+ optical clocks. This comprehensive approach, which integrates advanced laser stabilization techniques, precise experimental measurements, and rigorous theoretical modelling, aims to develop more reliable and accurate atomic clocks.

The findings of this work extend beyond just improving timekeeping. By deepening our understanding of how quantum systems interact with external fields, this research contributes to broader applications in quantum metrology and fundamental physics. The ability to precisely control and mitigate electric field-induced shifts has far-reaching implications for future technologies in quantum information and precision measurement.

Chapter 3

Experimental Setup

3.1 Electronics

The experimental setup for measuring the differential polarizability zero crossing of the Ba^+ ion relies heavily on precise electronic control systems to maintain the stability and accuracy of critical components. The key electronic subsystems include temperature control, current control, and high-voltage drivers for piezoelectric transducers (PZTs).

3.1.1 Temperature Control

Maintaining a stable temperature for components such as the External Cavity Diode Laser (ECDL), Tapered Amplifier (TA), and doubling cavity is crucial for consistent performance. Temperature fluctuations can lead to frequency drifts and instability in laser output.

- **Thermoelectric Coolers (TECs)**: TECs are commonly used for precise temperature regulation. By passing a controlled current through the TEC, heat can be absorbed or dissipated, allowing for fine temperature adjustments. This method effectively stabilises the temperature of laser diodes and optical components.
- **Temperature Controllers**: These devices monitor the temperature via sensors and adjust the current supplied to the TECs to maintain the desired setpoint. Implementing a Proportional-Integral-Derivative (PID) control algorithm ensures rapid response and minimal overshoot, leading to a stable operating environment for sensitive components.

3.1.2 Current Control

A stable current supply is vital for operating laser diodes and amplifiers, as fluctuations can cause output power and wavelength variations.

- **Laser Diode Drivers**: These circuits provide a constant current to the laser diode, ensuring stable light output. They often include feedback mechanisms that monitor the output power and adjust the current accordingly to maintain consistent performance.
- **Protection Features**: To safeguard laser diodes from damage due to current surges or overheating, drivers are equipped with slow-start circuits, current limiting, and over-temperature shutdown. These protections enhance the longevity and reliability of the laser system.

3.1.3 High-Voltage Driver for PZT

PZTs are used for fine adjustments in optical components, such as tuning the cavity length in ECDLs and doubling cavities. They require precise high-voltage control to achieve accurate positioning.

- **High-Voltage Amplifiers**: These devices amplify control signals to the voltage levels required by PZTs, ranging from tens to hundreds of volts. The amplifiers must deliver clean, stable voltage without introducing noise that could affect the system's precision.
- **Driver Circuit Design**: A typical PZT driver circuit includes a high-voltage operational amplifier configured to provide the necessary voltage range and current drive capability. The design ensures linear response and minimal distortion, critical for applications requiring precise control.

Incorporating these electronic control systems into the experimental setup ensures that the components operate within their optimal parameters, leading to accurate and reliable measurements of the Ba^+ ion's differential polarizability. These electronics' stability and precision are crucial for the experiment's success.

3.2 ECDL Laser

3.2.1 Overview

The External Cavity Diode Laser (ECDL) is a tunable laser system that offers a narrow linewidth using an external cavity formed by a diffraction grating. The ECDL operates in the Littrow configuration, where the diffraction grating reflects the first-order light back into the diode, forming an extended cavity. This helps achieve fine wavelength tuning and linewidth narrowing.

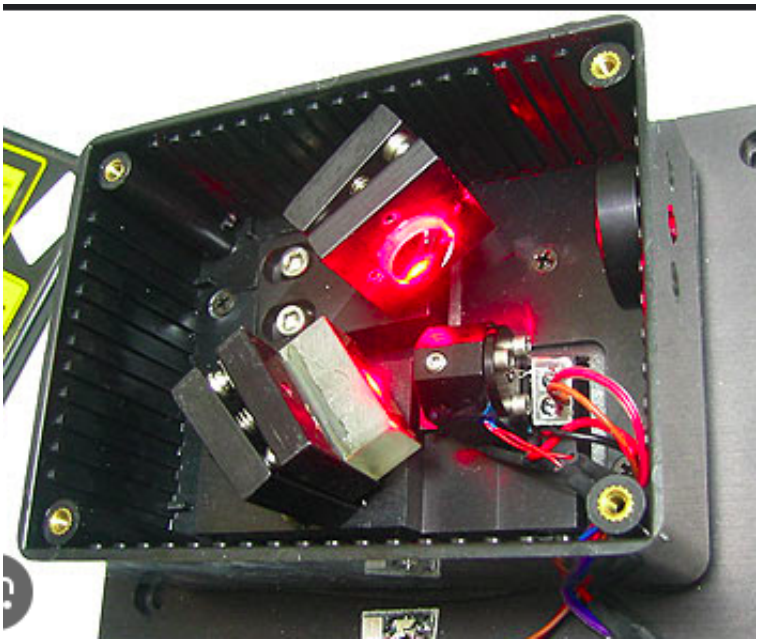

FIGURE 3.1: External Cavity Diode Laser.

3.2.2 Electronics of the ECDL Laser

Temperature Control

Temperature control is a critical component of the ECDL system, as even small temperature fluctuations can lead to frequency drifts, affecting laser stability.

Thermoelectric Coolers (TECs)

- **Function**: Thermoelectric coolers are used for precise temperature stabilization of the laser diode and the external cavity. TECs utilize the Peltier effect, which allows for heating or cooling depending on the direction of the electric current.
- **Operation**: The TECs are controlled by temperature controllers that use feedback from thermistors embedded in the laser housing. The TECs maintain a stable temperature by absorbing or dissipating heat.
- **Heat Management**: Applying a thin layer of thermally conductive paste between the TECs and the diode housing is crucial to ensure efficient heat transfer. This helps maintain a consistent temperature across the laser system.

Temperature Controllers

- **PID Control**: Temperature controllers use Proportional-Integral-Derivative (PID) control to maintain the temperature setpoint. The PID loop ensures rapid stabilization with minimal overshoot, essential for laser applications requiring high precision.
- **Setpoint Adjustment**: The temperature setpoint is typically adjusted to optimize the gain profile of the laser diode. Proper alignment of the diode's gain with the grating-selected wavelength is achieved by setting the temperature near the desired lasing wavelength, as detailed in the reference documents.

Current Control

The laser diode current must be precisely controlled to ensure stable output power and wavelength. Current fluctuations can lead to mode hops, significantly impacting the laser's performance.

Laser Diode Drivers

- **Constant Current Source**: The ECDL uses a constant current source to drive the laser diode, ensuring stable operation. The current must be adjusted carefully to avoid sudden jumps in the laser output (mode hops).
- **Current Tuning**: By varying the diode current, the internal modes of the laser can be shifted. This provides a means to fine-tune the wavelength around the target value, which is critical when aligning the laser to specific external modes.

Protection Mechanisms

- **Slow-Start Circuit**: A slow-start mechanism is implemented in the driver circuitry to protect the diode from sudden current surges. This reduces the risk of damage when powering on the system.
- **Over-Current Protection**: Zener diodes are used to prevent over-voltage, while Schottky diodes protect against reverse biasing of the laser diode. These protections are essential to prolong the life of the diode.

High-Voltage Driver for PZT

The diffraction grating in the ECDL is mounted on a piezoelectric transducer (PZT), which allows fine tuning of the external cavity length. The PZT is driven by a high-voltage amplifier, providing precise control over the cavity and, thus, the lasing frequency.

Piezoelectric Transducer (PZT)

- **Role in Frequency Control**: The PZT adjusts the external cavity length by changing the grating position, allowing frequency tuning. It can sweep the laser frequency over at least one external cavity's free spectral range (FSR).
- **Voltage Control**: The PZT requires a high-voltage driver, typically operating at 100 V or more, to achieve sufficient displacement for cavity length adjustments. This high-voltage input allows the grating angle to be adjusted over a wide range, facilitating precise alignment of the lasing mode.

High-Voltage Driver Circuit

- **Amplifier Design**: The high-voltage amplifier used for the PZT must have a clean, stable output without significant noise. Noise in the voltage signal can introduce a frequency jitter, affecting the stability of the laser.
- **Frequency Response**: The bandwidth of the PZT driver is typically limited to a few kilohertz, which makes it suitable for slow adjustments. Feedback is applied via the diode current rather than the PZT for fast adjustments.

3.2.3 Internal Workings of ECDL Laser

The Littrow Configuration

The ECDL operates in the Littrow configuration, where the diffraction grating reflects the first-order diffracted light back into the laser diode, thus forming an extended cavity. This configuration is chosen due to its simplicity and efficiency in wavelength selection, resulting in a significantly narrower linewidth.

Wavelength Tuning Mechanisms

Diffraction Grating Feedback The diffraction grating controls the wavelength of the laser by adjusting the grating angle:

$$m\lambda = d(\sin\theta_i + \sin\theta_d) \tag{3.1}$$

where m is the diffraction order, d is the groove spacing, θ_i is the incident angle, and θ_d is the diffracted angle.

PZT-Based Mechanical Tuning The PZT allows fine adjustments to the grating angle, providing precise wavelength tuning. The applied high voltage modifies the grating position to match the lasing wavelength with the desired external cavity mode.

Current Tuning Adjusting the injection current alters the refractive index of the diode, providing an additional means of fine wavelength tuning. This current-induced tuning is practical for minor wavelength adjustments and complements mechanical tuning.

Temperature Tuning Temperature tuning involves adjusting the operating temperature of the laser diode. Changing the temperature shifts the diode's bandgap energy and peak wavelength, providing coarse control over the laser wavelength.

Mode Selection and Linewidth Narrowing

Mode Competition The extended cavity created by the diffraction grating introduces mode competition, allowing only specific longitudinal modes to reach the lasing threshold. The feedback from the grating ensures **single-mode operation**.

Suppression of Spontaneous Emission The narrow linewidth of the ECDL results from the extended cavity suppressing spontaneous emission, effectively narrowing the range of allowed modes.

Stabilization Mechanisms

Feedback Control (PDH Locking) The laser frequency is stabilized using the **Pound-Drever-Hall (PDH) technique**. An electro-optic modulator (EOM) introduces phase modulation to the beam, which is then coupled to a reference cavity to generate an error signal for frequency stabilization.

Thermal and Acoustic Isolation The ECDL system is housed in a thermally and acoustically isolated environment to minimize fluctuations that could affect the laser frequency.

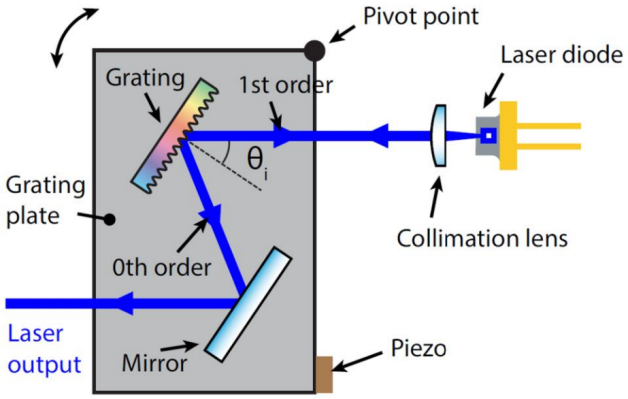

FIGURE 3.2: ECDL Schematic.

3.2.4 Advantages of ECDL Systems

The ECDL combines **narrow linewidth**, **broad tunability**, and **stable single-mode operation**, making it ideal for high-precision applications such as spectroscopy, atomic clocks, and quantum computing.

3.3 Triple Isolation After the ECDL Laser

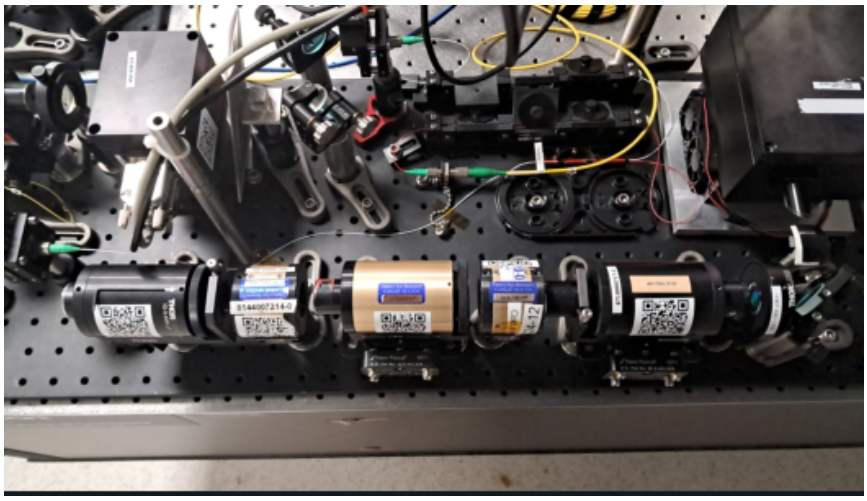

FIGURE 3.3: Triple Isolation.

3.3.1 Triple Isolation and Optical Feedback Protection

After the ECDL laser, **triple isolation** is employed to minimize the effects of unwanted optical feedback and to ensure the stability of the laser system. Using multiple isolators is critical to effectively eliminate potential back-reflections that could destabilize the laser, cause mode hops, or degrade the coherence and quality of the laser output.

Optical isolators allow light to pass in only one direction, effectively blocking any reflected light from re-entering the laser cavity. In high-precision experiments like this one, such reflections are a significant concern, as they can cause **fluctuations in the output frequency**, **power instability**, and **mode competition** in the laser cavity. Triple isolation ensures that the ECDL remains unaffected by these perturbations.

3.3.2 Purpose of Triple Isolation

- **Minimize Back-Reflections**: Any optical reflection travelling back into the laser cavity can interfere with the lasing process. Three isolators provide multiple attenuation stages, eliminating nearly all back-reflected light.
- **Maintain Single-Mode Stability**: Reflected light can interact with the extended cavity of the ECDL and cause unwanted mode hops. By employing three isolators, the stability of the single-mode operation is preserved, which is critical for applications requiring a narrow linewidth and high coherence.
- **Improvement in Signal Quality**: Triple isolation helps enhance the laser output's spectral purity, which is essential for precision measurements like those involving the zero-crossing determination of Ba^+ polarizability.

3.3.3 Challenges of Not Having Isolators in the Desired Range

One of the challenges faced in implementing the triple isolation setup was the **unavailability of optical isolators** with a sufficiently broad bandwidth or within the specific operating wavelength range required for the ECDL operating at **960 nm**.

3.3.4 How We Tackled the Problem

To tackle the problem of not having isolators of the desired range, several strategies were employed, including the use of an available **780 nm isolator** in combination with an **adjustable isolator**:

Using the 780 nm Isolator and Adjustable Isolator

- The **780 nm isolator** was used, even though it was not perfectly suited for the 960 nm operating wavelength of the ECDL. Despite the mismatch, the 780 nm isolator provided **22 to 23 dB of isolation** at 960 nm, which was effective to a certain extent in reducing back-reflections.
- To achieve the desired total isolation, an **additional adjustable isolator** was used, which provided another **22 dB of isolation**. Combining these two isolators achieved a sufficient level of isolation for stable operation.
- The combined setup, with isolation from the fixed and adjustable isolators, provided the required attenuation of back-reflected light, ensuring that the laser's output remained stable and free from unwanted mode hopping or instability.

Combining Isolators of Different Ranges

- Since isolators with the exact desired specifications were unavailable, the approach of combining the **780 nm isolator** with an adjustable isolator allowed us to create an effective isolation range that covered the **960 nm** wavelength used by the ECDL.
- This combination provided a total isolation of over **44 dB**, which was sufficient to effectively prevent any reflected light from affecting the laser cavity.

Using Broadband Polarizers

- **Broadband polarizers** were also used in conjunction with the isolators to further extend the effective operating range. These polarizers attenuated reflected light, especially in regions where the performance of the fixed isolator was not ideal.
- By placing a polarizer before and after the isolators, we improved the isolation effectiveness across the entire operating wavelength range.

Fine-Tuning the Laser Wavelength

- The **wavelength of the ECDL** was carefully fine-tuned to operate within the effective isolation range of the combined isolators. This involved precise adjustments of the grating angle, current, and temperature to ensure compatibility with the isolators' performance at 960 nm.

Tilted Optical Elements

- **Optical elements**, such as mirrors and beam splitters, were tilted to further mitigate back-reflections. By using slightly tilted optics, reflected beams did not travel directly back into the isolators or the laser cavity, which helped reduce the load on the isolators and minimized their limitations.
- This approach effectively reduced unwanted feedback without relying solely on the isolators, making the isolation more robust, even with sub-optimal components.

3.3.5 Summary of the Triple Isolation Solution

The triple isolation system protected against back-reflections, ensuring the ECDL operated with high stability. Despite not having isolators specifically designed for 960 nm, the combination of the **780 nm isolator** (providing 22 to 23 dB of isolation) and an additional **adjustable isolator** (providing another 22 dB of isolation) achieved the desired level of attenuation. The use of **broadband polarizers**, **fine-tuning of the laser wavelength**, and **tilted optical elements** further improved the robustness of the isolation system.

These measures ensured that the laser output remained stable, single-mode, and spectrally pure, which was crucial for the precision measurements required in the experiment. This adaptive approach provided the flexibility to utilize available components while achieving the desired level of isolation and stability for the laser system.

3.4 Tapered Amplifier (TA)

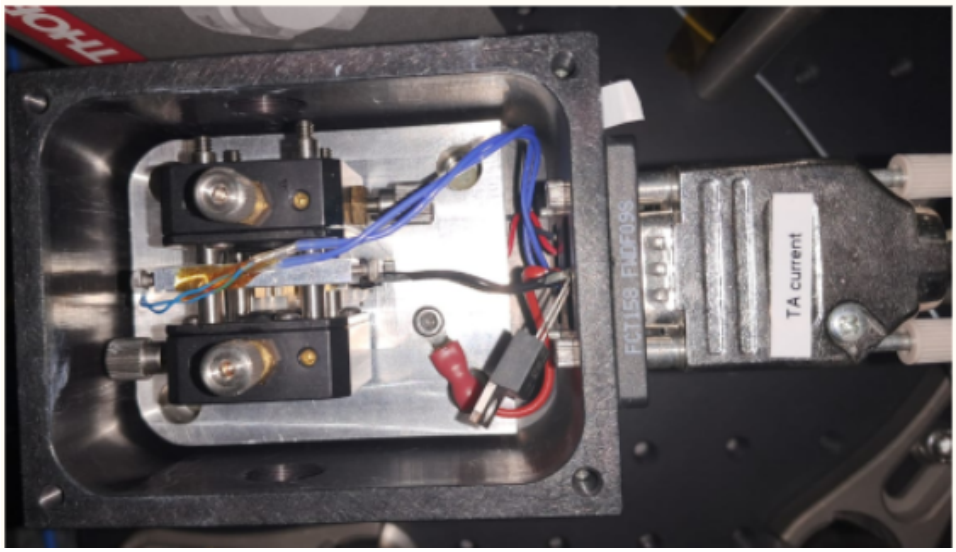

FIGURE 3.4: Tapered Amplifier.

3.4.1 Overview of Tapered Amplifier

The **Tapered Amplifier (TA)** is a critical component of the experimental setup used to boost the power of the laser output from the External Cavity Diode Laser (ECDL).

The TA offers high optical gain, amplifying the seed light while maintaining spectral characteristics, such as wavelength, linewidth, and coherence. This amplified light is subsequently used in various downstream processes, including **frequency doubling** and probing transitions in Ba^+ ions.

The TA operates by injecting a low-power, well-defined seed laser (in this case, from the ECDL) and amplifying it through a tapered gain medium, which provides a higher output power while maintaining the input wavelength's coherence properties.

3.4.2 Structure and Function

Tapered Gain Medium

- The **TA chip** is designed with a tapered gain region. The front section of the amplifier consists of a narrow waveguide, while the back end gradually expands into a tapered section.
- The **narrow waveguide** at the front allows for the efficient coupling of the seed light, while the **tapered section** increases the cross-sectional area, providing optical gain over a larger volume and reducing the risk of saturation.
- This design helps achieve amplification without compromising the quality of the output beam, as the seed laser's spectral properties are preserved.

Collimation Optics

- **Collimation lenses** are used at both ends of the TA to focus the seed laser into the narrow input section of the tapered amplifier and to collimate the output beam. This ensures efficient coupling and minimizes optical losses.
- The output beam is collimated and expanded as it leaves the TA, allowing for proper shaping for subsequent use.

3.4.3 Temperature Control of the TA

Temperature control is essential to ensure stable operation and efficient amplification within the TA. A **Proportional-Integral-Derivative (PID) controller** is used to regulate the amplifier's temperature.

- **Thermoelectric Coolers (TECs)** are used to stabilize the TA chip temperature. The gain medium operates efficiently by maintaining a stable temperature, minimizing the risk of thermal runaway, mode instability, and frequency drift.
- The **setpoint temperature** is adjusted based on the optimal operating conditions of the TA, typically at a point that provides maximum optical gain while reducing noise.

3.4.4 Current Control for Tapered Amplifier

The TA requires a significantly higher current than the ECDL to provide the desired level of optical amplification. The current supplied must be precisely controlled to maintain stable operation and avoid damaging the TA chip.

High-Current Driver

- The **high-current driver** supplies current to the TA, with the current typically in the range of **1 to 3 amps**, depending on the TA's specifications. This high current drives the gain medium and provides the necessary energy for amplification.
- **Stabilized Current Supply**: The current driver must provide a low-noise, stable current. Fluctuations in the current could lead to instability in the output power, affecting the overall stability of the experimental system.
- The high-current driver incorporates safety features like **current limiting** and **slow-start circuits** to protect the TA from damage due to excessive current or sudden surges.

3.4.5 Isolation Considerations

Since the TA amplifies the seed light, preventing any back-reflected light from reaching the TA and affecting its performance is critical.

- **Optical Isolators** are placed before and after the TA to ensure that back reflections do not enter the amplifier, which could destabilize the amplification process or cause damage to the TA chip.
- **Triple Isolation** before the TA is typically used to ensure that the seed light entering the TA is free of any back-reflected interference, maximizing the amplification quality.

3.4.6 Alignment and Coupling

Proper alignment of the seed light into the TA is crucial for efficient amplification. Misalignment can lead to lower gain, degraded beam quality, or damage to the TA chip.

Beam Coupling

- The seed laser is coupled into the TA using precise optics to ensure the beam is well-aligned with the input facet of the TA chip. This is typically done using an adjustable mount to fine-tune the alignment.

Optimization Procedure

- The output power of the TA is monitored during alignment to ensure maximum coupling efficiency. Fine adjustments to the coupling optics are made to achieve optimal alignment, maximizing the gain while maintaining good beam quality.

3.4.7 Output Power and Beam Quality

The TA provides significantly increased output power compared to the input seed, typically amplifying it to a level suitable for further applications such as frequency doubling.

Power Levels

- The output power can range from **several hundred milliwatts to a few watts**, depending on the current supplied and the characteristics of the TA.

Beam Quality

- The TA is designed to maintain the spatial mode of the seed laser, providing an output beam with good coherence properties. The beam is typically **Gaussian-shaped** and has a low divergence, making it ideal for subsequent stages in the experimental setup.

3.4.8 Safety Considerations

Operating a Tapered Amplifier requires careful handling due to the high power levels and currents.

Thermal Management

- Proper heat sinking is essential to dissipate the heat the TA generates. Without adequate thermal management, the TA chip could overheat, leading to reduced performance or damage.

Current Limiting and Shutdown

- The current driver is equipped with features to limit the maximum current and to shut down in case of overheating or overcurrent situations. This helps protect the TA chip from accidental damage.

3.4.9 Summary of Tapered Amplifier Functionality

The Tapered Amplifier in the experimental setup provides the high-power output necessary for downstream processes while maintaining the spectral properties of the ECDL seed laser. The combination of **temperature control**, **high-current stable drive**, **precise alignment**, and **isolation measures** ensures that the TA operates efficiently and reliably. The amplified beam retains high coherence and low divergence, making it suitable for frequency doubling and probing the Ba^+ ion transitions.

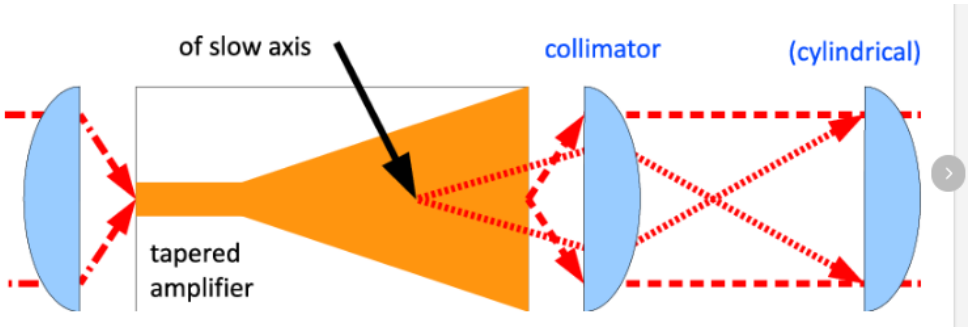

FIGURE 3.5: Tapered Amplifier Schematic.

3.5 Doubling Cavity

3.5.1 Overview of Doubling Cavity

The **Doubling Cavity** is a key component in the experimental setup, used to convert the fundamental wavelength of the laser into its second harmonic. In the context of the Ba^+ polarizability experiment, the doubling cavity is used to generate **480 nm light** by **frequency doubling** the output of the **960 nm** laser from the Tapered Amplifier (TA). This process is essential for probing transitions in Ba^+ ions. Using a **PPKTP crystal** ensures efficient frequency doubling, with an achieved efficiency of **45% to 50%**.

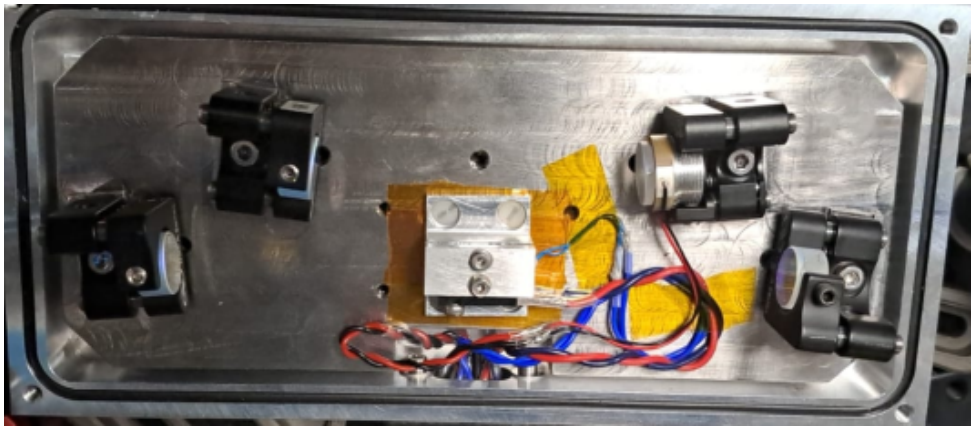

FIGURE 3.6: Doubling Cavity.

3.5.2 Structure of the Doubling Cavity

Nonlinear Crystal: PPKTP

- The **PPKTP crystal** is the core of the doubling cavity, where the second-harmonic generation (SHG) takes place. PPKTP is used because of its **high nonlinear coefficient**, **low absorption** at both the fundamental (960 nm) and second harmonic (480 nm) wavelengths, and the ability to achieve **quasi-phase matching**.
- **Periodically Poled Structure**: The PPKTP crystal is periodically poled to achieve quasi-phase matching, allowing for efficient conversion of the fundamental wavelength to the second harmonic. The periodic poling structure compensates for the natural dispersion in the crystal, maximizing the SHG efficiency.

High-Finesse Optical Cavity

- The **optical cavity** is formed by mirrors surrounding the nonlinear crystal to create a **standing wave** of the fundamental laser light.
- The cavity is designed to enhance the intensity of the fundamental wavelength within the PPKTP crystal, increasing the efficiency of the frequency doubling process. The cavity mirrors are **highly reflective** for the **960 nm light** and **anti-reflective** for the **480 nm light** to allow the second harmonic to be coupled out efficiently.

Temperature Control of PPKTP Crystal

- The temperature of the PPKTP crystal is stabilized using a **temperature-controlled oven**. The temperature must be precisely controlled to maintain **quasi-phase matching**, critical for efficient frequency conversion.
- **Temperature Phase Matching**: The PPKTP crystal's refractive index changes with temperature, and by maintaining the crystal at the optimal temperature, efficient phase matching for SHG is achieved. For PPKTP, this temperature is typically in the range of **40°C to 80°C**, depending on the periodic poling period.

3.5.3 Cavity Stabilization

Stabilizing the doubling cavity is essential for maintaining resonance with the fundamental wavelength. The **Pound-Drever-Hall (PDH) locking** technique is employed for stable resonance.

Pound-Drever-Hall (PDH) Locking Technique

- **Electro-Optic Modulator (EOM)**: The laser light is phase-modulated using an EOM before entering the cavity, creating sidebands around the carrier frequency.
- **Error Signal Generation**: The light reflected from the cavity is detected and mixed to generate an error signal, which provides information about the resonance condition of the cavity.
- **Feedback Loop**: The error signal is fed back to a **Piezoelectric Transducer (PZT)** attached to one of the cavity mirrors. This feedback is used to make fine adjustments to maintain resonance between the cavity and the fundamental wavelength, thus maximizing the intensity of the 960 nm light inside the cavity and enhancing the second-harmonic output.

Automatic Lock Acquisition

- An **auto-lock system** ensures that the cavity remains locked even if environmental disturbances cause it to lose resonance.
- The **auto-lock** system continuously monitors the error signal and re-engages the lock if needed, ensuring consistent second-harmonic generation during extended experimental runs.

3.5.4 High Voltage Driver for PZT

The PZT plays a significant role in maintaining the cavity length at resonance with the fundamental frequency.

- **Cavity Length Control**: The PZT adjusts the position of one of the mirrors to keep the cavity length in resonance with the fundamental wavelength. A **high-voltage driver** is used to provide the necessary voltage to move the PZT, allowing for precise control over the cavity length.
- **Bandwidth and Response**: The PZT driver has a high bandwidth to respond quickly to error signal changes, ensuring optimal frequency doubling conditions.

3.5.5 Phase Matching and Efficiency Optimization

Quasi-Phase Matching in PPKTP

- **Temperature Control for Phase Matching**: The temperature of the PPKTP crystal is maintained to achieve optimal quasi-phase matching conditions. Temperature control allows the crystal's refractive index to match the conditions needed for efficient conversion of the fundamental wavelength to its second harmonic.
- **Periodic Poling**: The PPKTP crystal has a periodically poled structure, allowing the crystal to achieve **quasi-phase matching** without birefringence. This structure compensates for the natural dispersion and maintains a consistent phase relationship between the fundamental and second-harmonic waves, leading to high efficiency.

Cavity Alignment

- **Initial Alignment**: The mirrors of the doubling cavity are aligned so that the fundamental beam passes through the nonlinear crystal along the optimal axis for phase matching.
- **Optimization Procedure**: The alignment is adjusted while monitoring the output power of the second harmonic. Fine adjustments to the mirror positions and crystal orientation are made to maximize the output, achieving a frequency doubling efficiency of **45% to 50%**.

3.5.6 Output Coupling and Filtering

The second-harmonic light generated in the cavity must be separated from the fundamental light and directed towards the experimental setup.

- **Output Coupler**: The output coupler mirror is **anti-reflective** for the second harmonic (480 nm) and **highly reflective** for the fundamental wavelength (960 nm). This ensures efficient coupling of the generated 480 nm light out of the cavity.
- **Filtering**: A **dichroic mirror** further separates the residual fundamental light from the second harmonic. This ensures that only pure 480 nm light is used for subsequent experimental stages.

3.5.7 Safety and Thermal Management

Due to the high circulating power within the doubling cavity, thermal management and safety precautions are necessary to ensure stable operation.

- **Heat Dissipation**: The high power density inside the cavity can lead to heating of the PPKTP crystal. To manage this, a **thermally conductive baseplate** is used to dissipate heat and prevent damage to the crystal.
- **Power Monitoring**: Power sensors are placed strategically in the setup to continuously monitor the output power levels. Any significant deviation in power can indicate alignment issues or phase mismatch, allowing prompt corrective action.

3.5.8 Summary of Doubling Cavity Functionality

The doubling cavity is integral to converting the **960 nm fundamental light** from the Tapered Amplifier into **480 nm light** for probing Ba^+ ion transitions. The use of a **PPKTP crystal** with **periodic poling** provides efficient frequency doubling through quasi-phase matching, with an achieved conversion efficiency of **45% to 50%**. The combination of a **high-finesse optical cavity**, **temperature control**, and **Pound-Drever-Hall (PDH) locking** ensures optimal phase matching and high-efficiency second-harmonic generation. These features enable stable, high-power output, which is essential for precision atomic measurements.

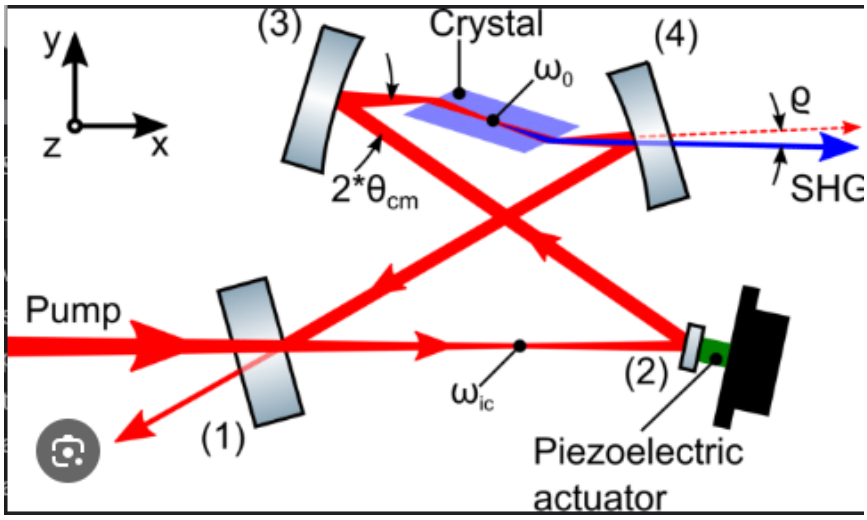

FIGURE 3.7: Doubling Cavity Schematic.

3.6 Pound-Drever-Hall (PDH) Locking Technique

3.6.1 Overview of PDH Locking Technique

The **Pound-Drever-Hall (PDH) locking technique** is an essential method used to stabilize the laser frequency with respect to an optical cavity. In the doubling cavity setup, PDH locking ensures that the **fundamental wavelength** remains resonant within the cavity, thereby enhancing the intensity inside the cavity and maximizing the efficiency of the **frequency doubling process**. This stabilization method is crucial for maintaining consistent second-harmonic generation and ensuring the cavity operates optimally.

3.6.2 Basic Principle of PDH Locking

The PDH technique involves creating an **error signal** that indicates the detuning between the laser frequency and the resonant frequency of the cavity. This error signal is then used to adjust the cavity length or laser frequency to keep the system locked to resonance.

Electro-Optic Modulator (EOM) and Phase Modulation

- A **phase modulation** of the laser light is performed using an **Electro-Optic Modulator (EOM)**. The EOM adds small frequency sidebands around the laser

carrier frequency by modulating the phase at a fixed modulation frequency, typically in the range of **a few MHz**.

- The modulation produces sidebands that generate an error signal without affecting the main laser power in the cavity.

Cavity Reflection and Error Signal Generation

- The modulated laser beam is sent to the **doubling cavity**, and the portion of the light that does not enter the cavity (due to detuning) is reflected.
- The reflected light is then detected using a **fast photodiode**. The photodiode detects interference between the reflected carrier and sidebands, producing a signal that contains information about the resonance condition.
- This signal is mixed with the original modulation frequency using a **mixer** to generate the **PDH error signal**. The error signal is a **DC signal** that indicates the frequency detuning between the laser and the cavity resonance.

Feedback Control Loop

- The error signal is fed back to a **Piezoelectric Transducer (PZT)** attached to one of the cavity mirrors. The PZT adjusts the mirror position, changing the cavity length to match the laser frequency and keep the system in resonance.
- In some setups, the error signal may also be used to adjust the **laser diode current**, providing an additional fast feedback path for laser frequency control.

3.6.3 Implementation of PDH Locking in Doubling Cavity

In the **doubling cavity** setup, the PDH locking technique is implemented to achieve a stable resonance of the **960 nm fundamental light** within the cavity. The components involved include:

- **Electro-Optic Modulator (EOM)** for phase modulation of the laser beam.
- **Fast Photodiode** for detecting reflected light and generating a signal that contains information about the cavity detuning.
- **Mixer** to demodulate the detected signal and produce the PDH error signal.
- **PZT Driver** to actuate the PZT and control the cavity length.
- **Servo Controller** to process the PDH error signal and provide appropriate feedback to the PZT and/or laser current driver.

This feedback system allows the cavity to maintain resonance with the laser, thereby enhancing the power circulating inside the cavity and improving the efficiency of the frequency-doubling process.

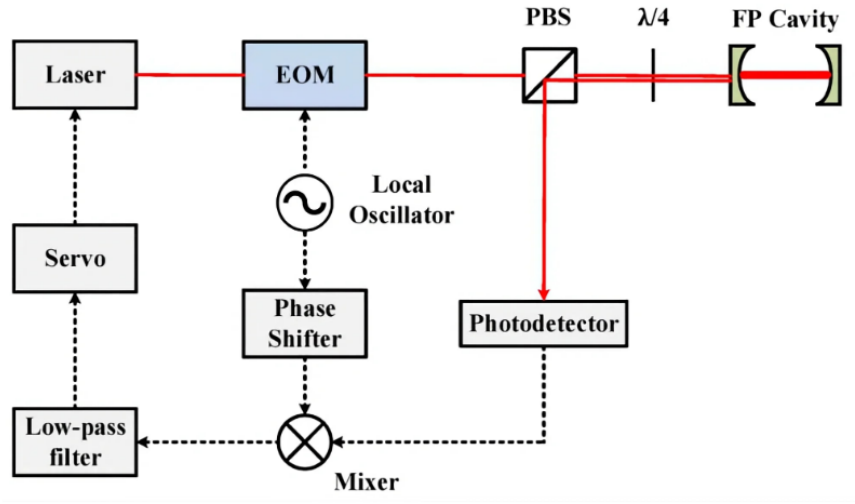

FIGURE 3.8: PDH Lock Schematic.

3.7 Autolock Circuit Implementation

3.7.1 Purpose of the Autolock Circuit

The **autolock circuit** is designed to monitor the lock condition and automatically restore the lock if it is lost due to any external disturbances. This is particularly important for long-term stability and continuous operation of the doubling cavity in the experiment.

3.7.2 Components of the Autolock Circuit

The auto-lock circuit consists of the following key components:

- **Microcontroller or Logic Circuit**: Used to monitor the lock's status by evaluating the error signal level.
- **Relay or Switch**: Used to engage or disengage the locking loop. When the lock is lost, the auto lock circuit temporarily breaks the feedback loop, allowing the system to reset before attempting to regain the lock.
- **Lock Detector**: This is usually implemented by monitoring the amplitude of the **error signal**. The lock has been lost when the error signal exceeds a certain threshold.

3.7.3 Working of the Autolock Circuit

Monitoring the Lock Status

- The auto lock circuit continuously monitors the **error signal** output from the PDH setup. The system loses the lock if the error signal exceeds a predefined threshold.
- The **lock detector** triggers the auto lock process if the error signal deviates significantly from zero, which is the condition for being in resonance.

Breaking the Feedback Loop

- When the auto lock circuit detects a loss of lock, it disengages the feedback loop by momentarily **cutting the control voltage** supplied to the PZT. This is done using a **relay or electronic switch**.
- Breaking the feedback loop allows the system to reset and prevents the PZT from attempting to make large corrections, which could destabilize the system further.

Re-Engaging the Lock

- After a brief pause, the circuit re-engages the feedback loop by restoring the control voltage. The **servo controller** then attempts to bring the cavity back into resonance by controlling the PZT or adjusting the laser current.
- If the initial attempt fails, the auto lock circuit continues this cycle until the lock is successfully re-established.

3.7.4 Optimizing the Autolock Parameters

- The **response time** of the auto lock circuit is carefully optimized to minimize the time taken to regain the lock without causing excessive wear on the PZT or creating instability.
- The **threshold level** for detecting a loss of lock is adjusted to balance sensitivity and robustness, ensuring that the system only triggers the auto lock process in the event of significant disturbances rather than minor fluctuations.

3.7.5 Summary of PDH Locking and Autolock Implementation

The **Pound-Drever-Hall (PDH) locking technique** provides precise control of the laser frequency and cavity resonance, ensuring efficient second-harmonic generation in the doubling cavity. The use of an **EOM** for phase modulation, a **fast photodiode** for error signal detection, and a **PZT** for cavity length adjustment creates a stable feedback system.

The **autolock circuit** further enhances the stability of the setup by automatically restoring the lock when external disturbances cause the system to lose resonance. This automated feature is critical for maintaining long-term stability and ensuring continuous operation during experimental runs, particularly when the doubling cavity is used for high-precision measurements.

3.8 Double Path Acousto-Optic Modulator (AOM) and Switching Mechanism

3.8.1 Overview of Acousto-Optic Modulator (AOM)

An **Acousto-Optic Modulator (AOM)** is an essential component for manipulating laser beams in an optical system. The AOM exploits the acoustic-optic effect, where an acoustic wave creates a refractive index grating within a crystal. This grating diffracts the incident laser beam, and the intensity and direction of the diffracted beam can be manipulated by controlling the acoustic wave.

In the **double path configuration**, the AOM allows for enhanced control of the laser power and provides precise on/off switching of the laser beam, which is crucial for many aspects of the experiment, such as frequency doubling, stabilization, and probing atomic transitions.

3.8.2 Double Path Configuration of AOM

The **double path AOM** setup involves passing the laser beam through the AOM twice to achieve better extinction ratios and more efficient power modulation. This configuration provides greater flexibility and control over the output laser beam.

How the Double Path Works

- **First Pass through AOM**: The laser beam is passed through the AOM, which is diffracted into several orders. Typically, the **first-order** diffraction is used for subsequent operations, while the **zero-order** beam is blocked or diverted from the optical path.
- **Second Pass for Enhanced Modulation**: After the first diffraction, the first-order beam is redirected back through the AOM a second time. This second pass through the AOM results in improved diffraction efficiency and a **higher extinction ratio** compared to a single-pass configuration.
- **Beam Recombination**: The double-pass configuration effectively cancels out any phase shifts or beam walk-off that may have been introduced in the first pass, leading to better alignment and consistency of the output beam.

3.8.3 Advantages of the Double Path AOM

- **Enhanced Extinction Ratio**: The double path AOM provides an improved **extinction ratio** of the laser beam, which is particularly beneficial for precise experiments where the residual light must be minimized.
- **Greater Power Modulation**: By passing through the AOM twice, the modulation depth increases, allowing for more accurate laser power control.
- **Stability and Alignment**: The double pass cancels out any positional shifts caused by the first pass, resulting in a more stable and aligned output beam.

3.8.4 Switching Mechanism for the Double Path AOM

The **switching mechanism** for the AOM allows precise control over whether the laser beam is transmitted through the system or blocked. This switching capability is crucial for time-resolved measurements, frequency locking, and other experiment aspects requiring precise laser control.

RF Driver for Acoustic Wave Generation

- The AOM is controlled by an **RF (Radio Frequency) driver**, which generates an acoustic wave within the AOM crystal.
- The **frequency** of the RF signal determines the diffraction angle of the beam, while the **amplitude** of the RF signal controls the intensity of the diffracted beam. The AOM can effectively act as a fast switch for the laser beam by modulating the RF signal.

Fast Switching Capability

- **Turn-On/Off Speed**: The AOM provides very fast switching times, typically on the order of **nanoseconds to microseconds**. This fast response time is crucial for applications requiring precise timing, such as probing atomic transitions or implementing feedback loops for stabilization.
- **Pulse Generation**: The switching mechanism of the AOM allows it to create well-defined **pulses** of laser light by turning the RF signal on and off. The pulse duration can be adjusted by controlling the RF modulation, enabling the creation of laser pulses with adjustable duration and repetition rates.

Implementation in the Experimental Setup

- The AOM is positioned in the laser path after the **Tapered Amplifier (TA)**, where the beam is sufficiently amplified for the desired downstream processes.
- The double path setup is configured such that the beam passes through the AOM twice, maximizing the modulation depth and minimizing any residual zero-order leakage that might interfere with the experiment.

3.8.5 Feedback Control with AOM

- The AOM is also used in feedback loops to **stabilize the power** of the laser beam in the cavity. By monitoring the power of the laser beam after the AOM, the RF signal can be modulated to adjust the beam power in real time.
- This feedback capability ensures that the laser power remains consistent, which is critical for maintaining resonance within the **doubling cavity** and optimizing second-harmonic generation efficiency.

3.8.6 Safety Considerations

- **Over-Drive Protection**: The AOM RF driver is equipped with a protection mechanism to prevent **over-driving** of the AOM crystal, which could cause heating and damage.
- **Thermal Management**: The AOM crystal, when driven at high RF power, can generate heat. **Heatsinks** or active cooling systems are employed to dissipate this heat and maintain the crystal at an optimal operating temperature.

3.8.7 Summary of Double Path AOM and Switching Mechanism

The **double path AOM** and its **switching mechanism** provide precise control over the laser beam in the experimental setup. Bypassing the beam through the AOM twice, an enhanced extinction ratio and more significant power modulation are achieved, ensuring stability and precision. The **RF driver** controls the AOM, providing fast switching capabilities essential for time-sensitive experiments and feedback stabilization. This system allows for real-time control of the laser beam power, helping to maintain resonance within the doubling cavity and improving overall efficiency in second-harmonic generation.

Implementing the double path AOM setup, with its fast switching and high modulation depth, makes it a versatile tool for controlling the laser beam throughout the experiment, ensuring the accuracy and stability of the laser's interactions with the atomic system.

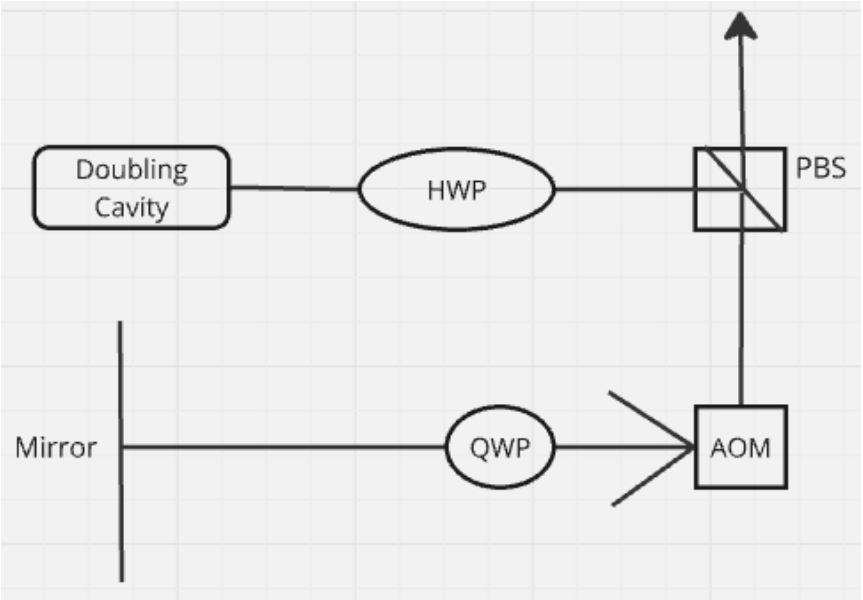

FIGURE 3.9: AOM Switch Schematic.

Chapter 4

Discussion

4.1 Overview of the Achievements

The current experimental setup for measuring the **polarizability zero crossing** in Ba^+ ions at **480 nm** represents significant progress in terms of both infrastructure and methodology. The various components of the setup, including the **External Cavity Diode Laser (ECDL)**, **Tapered Amplifier (TA)**, **Doubling Cavity**, and **Double Path Acousto-Optic Modulator (AOM)**, have been meticulously assembled and characterized to ensure stable and high-quality laser operation. Each component has been carefully calibrated to achieve the desired precision and stability required for the experiment.

4.2 Key Achievements in Setup and Stability

- **Temperature Control and Laser Stabilization**: The **ECDL** and the **TA** were optimized for maximum stability. Temperature stabilization using **Thermoelectric Coolers (TECs)** and **PID controllers** has resulted in a consistent output frequency, essential for accurate polarizability measurements.
- **High-Quality Frequency Doubling**: The implementation of the **PPKTP crystal** in the **Doubling Cavity** achieved an efficiency of **45% to 50%** for converting the fundamental **960 nm light** into **480 nm light**. This efficiency is crucial for probing the Ba^+ ion transitions and supports the ultimate goal of understanding the differential polarizability at the zero crossing.
- **Enhanced Control through Double Path AOM**: The **Double Path AOM** provided improved power modulation and switching capabilities, ensuring that the laser beam used for experiments is stable, precise, and capable of handling rapid modulation requirements. This capability is particularly beneficial for future measurements, which demand stringent laser beam intensity and timing control.
- **Precision Locking using PDH Technique**: The **Pound-Drever-Hall (PDH) locking** system for stabilizing the doubling cavity has been successfully implemented. This system ensures that the fundamental laser wavelength remains resonant within the cavity, enhancing the power density and, thus, the efficiency of the frequency doubling process.

4.3 Challenges Encountered and Overcoming Them

Several challenges were encountered during the setup and have been tackled effectively:

- **Lack of Desired Isolators**: During the setup, the **optical isolators** for **960 nm** were not readily available. To overcome this issue, a **780 nm isolator** was used, which provided partial isolation of **22 to 23 dB**. This isolation was further enhanced by using an **adjustable isolator** to achieve an additional **22 dB** of isolation. The combined approach successfully mitigated the risk of back-reflections into the laser source, which could have impacted stability.
- **High Voltage Driver Stability**: The high-voltage drivers used for the **PZT** in the doubling cavity and the ECDL setup had to be optimized to minimize noise and ensure smooth cavity tuning. This was particularly important for the **PDH lock** to operate effectively, and considerable effort went into isolating noise sources and ensuring clean voltage supplies.

4.4 Expected Outcomes

With the experimental setup now fully constructed and operational, the next phase of the project will focus on conducting measurements to determine the **polarizability zero crossing** at **480 nm** in Ba^+ ions. The expected outcomes include:

- **Accurate Determination of Zero Crossing**: By conducting high-precision measurements, the differential polarizability at the **480 nm zero crossing** will be determined. This measurement is crucial for understanding the interaction between Ba^+ ions and external electric fields, specifically how these interactions contribute to Stark shifts.
- **Validation of Theoretical Models**: The experimental measurements will be compared with the theoretical models discussed earlier in the report. The **zero crossing measurements** will provide critical insights into the accuracy of the differential polarizability model and help refine parameters such as branching ratios and matrix elements.

4.5 Challenges Anticipated During Measurements

Although the setup is complete, several challenges are anticipated during the measurement phase:

- **Environmental Stability**: Polarizability measurement requires extreme stability, free from mechanical vibrations and temperature fluctuations. Despite implementing several stabilization techniques, the experimental area must be kept isolated from external disturbances during the measurement phase.
- **Residual Light Management**: Even with a high extinction ratio provided by the **double path AOM**, managing **residual light** remains a challenge. Residual light can contribute to background noise, affecting the precision of polarizability measurements. Additional filtering and isolation might be required during measurements to ensure signal purity.

- **Maintaining Cavity Resonance**: Ensuring the **doubling cavity** remains in resonance during extended measurement periods could pose challenges due to thermal drifts or long-term piezoelectric creep. The **autolock mechanism** will play a critical role in maintaining resonance, but its effectiveness must be closely monitored.

4.6 Future Prospects

The successful completion of the measurements will provide a comprehensive understanding of the **polarizability behaviour** of Ba^+ ions at the **480 nm wavelength**. This, in turn, has several potential applications:

- **Improving Atomic Clock Precision**: The findings from this experiment are expected to contribute to the development of **more accurate optical frequency standards** by mitigating electric field-induced shifts. The knowledge gained from this study can be directly applied to reducing **Stark shifts** in Ba^+ based atomic clocks, thus improving their precision.
- **Contribution to Fundamental Physics**: The study of differential polarizability and its dependence on various parameters also provides insights into **atom-light interactions**, contributing to broader applications in **quantum metrology** and **fundamental research**. The high-precision models developed and validated in this work can be used in other experiments involving ion trapping, quantum information, and spectroscopy.

4.7 Summary

In summary, the experimental setup for the **Ba^+ polarizability zero crossing** measurement at **480 nm** is now operational, with all major components calibrated and optimized for the next phase of data acquisition. The setup includes a stable **ECDL and TA**, a high-efficiency **doubling cavity** with **PPKTP crystal**, precise modulation using a **double path AOM**, and robust stabilization via **PDH locking** and **autolock mechanisms**. While challenges have been encountered and effectively managed during the setup phase, further obstacles are expected during the actual measurement phase, primarily related to environmental stability and maintaining long-term resonance.

The comprehensive infrastructure and methodologies developed in this project are expected to yield high-precision results, ultimately advancing our understanding of the **differential polarizability** of Ba^+ ions and contributing significantly to the field of **atomic metrology** and **quantum measurements**.

Bibliography

Arnold, K. J. et al. (2019). "Measurements of the branching ratios for 6P1/2 decays in 138Ba+". In: *arXiv preprint arXiv:1905.06523*.

Barrett, M. D., K. J. Arnold, and M. S. Safronova (2019). "On the polarizability assessments of ion-based optical clocks". In: *arXiv preprint arXiv:1905.04976*.

Chanu, S. R. et al. (2020). "Magic wavelength of the 138Ba+ 6s 2S1/2 – 5d 2D5/2 clock transition". In: *Physical Review A* 101, p. 042507.

Hoffman, Matthew et al. (2013). "Radio-frequency-spectroscopy measurement of the Lande g(J) factor of the 5D(5/2) state of Ba+ with a single trapped ion". In: *Physical Review A* 88.2, p. 025401.

Le Kien, Fam, Philipp Schneeweiss, and Arno Rauschenbeutel (2013). "Dynamical polarizability of atoms in arbitrary light fields: general theory and application to cesium". In: *The European Physical Journal D* 67, p. 92.

Zhang, Zhiqiang et al. (2020). "Branching fractions for $P_{3/2}$ decays in Ba^+". In: *Physical Review A* 101, p. 062515.